

Localized convection in rotating stratified fluid

J. A. Whitehead

Department of Physical Oceanography, Woods Hole Oceanographic Institution, Woods Hole, Massachusetts

J. Marshall

Department of Earth, Atmospheric and Planetary Science, Massachusetts Institute of Technology, Cambridge, Massachusetts

G. E. Hufford

Woods Hole Oceanographic Institution, Massachusetts Institute of Technology Joint Program, Cambridge, Massachusetts

Abstract. We study the convective overturning of a rotating stratified fluid in the laboratory. Convection is induced from the surface of a salt-stratified fluid by the introduction of salty fluid over a circular area. The external parameters are buoyancy forcing of strength, B_0 , applied over a circular area of radius R_s , the rotation rate as measured by f , ambient stratification N , and the depth H . The experiments are motivated by physical scaling arguments which attempt to predict the length and velocity scales of the convective chimney as it adjusts under gravity and rotation and breaks up through baroclinic instability. The scales of interest include the number, size, and typical speeds of the fragments of the broken chimney, the final depth of penetration of the convective mixed layer, and the total volume of convectively produced water. These scales are tested against the laboratory experiments and found to be appropriate. In this idealized problem we have found the depth of penetration depends only on the size and strength of the forcing and the ambient stratification encountered by the convection event; it does not depend explicitly on rotation. The implications of the work to deep water formation in the Labrador Sea and elsewhere are discussed. Finally, the study has relevance to the role and representation of baroclinic eddies in large-scale circulation of the ocean.

Introduction

That deep water in the oceans is cold, and the deepest water is the coldest, has been known since the 18th century [Ellis, 1751], although salinity can complicate this simple picture [Veronis, 1972]. In general, the oceans are stably stratified everywhere, except in top and bottom mixed layers; even polar oceans are stably stratified in spite of the fact that the coldest water is created there and sinks downward to spread out to temperate and tropical latitudes. Thus surface cooling/evaporation/ice formation do not frequently directly produce water that is denser than the deepest water in the region. Instead, in polar oceans the dense water “makes its way” downward by two different routes: by flowing downward as density currents along the continental slope from areas of origin in shallow seas [see e.g., Nansen, 1906], [Gawarkiewicz and

Chapman, 1995]; or, in the open ocean, by deep convection events which are manifested as a very deep mixed layer induced by wintertime buoyancy loss [Stommel, *et al.*, 1971]. The latter process is the focus of this study.

Deep ocean convection is apparently only found in regions that are preconditioned regions, where gyre-scale and mesoscale circulation have weakened the ambient stratification sufficiently for rapid cooling/evaporation/freezing to produce very deep mixed layers during periods of maximum cooling in winter. During the formation of the deep mixed layer, water moves vertically with velocities of 2–10 cm s⁻¹ within the deep mixed layer [Stommel *et al.*, 1971; Schott and Leaman, 1991]. The vertical movement is both upward and downward and is recorded episodically by current meters; these individual convection cells have become known as plumes, and they act to efficiently “mix” the layer. The mixed layer depth increases from hundreds of meters to possibly thousands of meters over the period of a few days. After and possibly during the latter stages of the deep mixed layer formation, the entire volume of mixed-layer fluid sinks by spreading laterally at its base and contracting laterally at the surface. Simultaneously, the

Copyright 1996 by the American Geophysical Union.

Paper number 96JC02322.
0148-0227/96/96JC-02322\$09.00

sides of the deep mixed layer develop geostrophic eddies which augment this sinking.

Many theoretical, numerical, and laboratory modeling studies have clarified the dynamics of such deep ocean convection events. *Killworth* [1976]; *Crépon et al.* [1989], and *Madec et al.*, [1991], for example, focused upon generation of a large-scale flow while parameterizing the convective scale. The dynamics of adjustment with the surrounding stratified fluid and the production of eddies along the region dividing the cooled and uncooled fluid were topics of interest. The cooling was regarded as a distinct event with the lateral adjustment processes happening concurrently. Linear theory of rotating Rayleigh-Bénard convection summarized in the work by *Chandrasekhar* [1961] was employed to address the dynamics of the plumes. *Davey and Whitehead* [1981], for example, showed that convection cells wider than an appropriately defined Rossby radius of deformation $(g\Delta\rho H/\rho_0)^{1/2}/f$ would not grow, where g is acceleration from gravity, $\Delta\rho/\rho$ is the proportion of vertical density variation (but an adverse density gradient, with densest water on the surface), H is depth of the fluid layer, and f is the Coriolis parameter. *Fernando et al.* [1991] and *Bubnov and Golitsyn* [1990], used scaling arguments to explore the nonlinear regime, determined the region of parameter space where rotation was dominant, and produced information about the length and velocity scales within that region. *Fernando, et al.*, [1991] identified the length scale

$$l_{\text{rot}} = (B_0/f^3)^{1/2} \quad (1)$$

such that the critical depth, found experimentally to be $12.7 l_{\text{rot}}$, is the boundary layer thickness beyond which rotation becomes important in steady convection. The significance of l_{rot} is that for distances greater than l_{rot} the effects of rotation are important whereas for smaller distances rotation is not. Typically, in the ocean, l_{rot} is about 100 m. Here B_0 is buoyancy flux defined for heating or cooling as $B_0 = g\alpha H_f/\rho c_p$, where g is acceleration of gravity, α is the coefficient of thermal expansion, H_f is the heat flux per unit area, ρ is density, and c_p is specific heat, respectively. For salt flux, $B_0 = g\beta F_s$, where β is the salt coefficient of expansion and F_s is the volume flux of salt. *Maxworthy and Narimousa* [1991, 1994] presented evidence in support of the importance of l_{rot} and introduced the associated dimensionless "natural" Rossby number defined in terms of external parameters

$$R_0^* = l_{\text{rot}}/H. \quad (2)$$

In addition, a new length scale, a radius of deformation,

$$l_\rho = H(R_0^*)^{1/2} \quad (3)$$

was found to determine the diameter of groups of individual thermals that aggregated on the bottom in closed cells.

Numerical studies by *Jones and Marshall* [1993] have also supported the scalings tested by *Maxworthy and Narimousa* [1991, 1994] in the laboratory. Using nonhydrostatic models, they focused on both the production of the small-scale convection cells and the emergence of the larger aggregate scale in which lumps of cold water cluster together. *Legg and Marshall* [1993] found that the lumps of dense water tended to pair up with corresponding gyres of cyclonic surface fluid to produce "heton" pairs, which move the dense fluid laterally from the place of origin.

Helfrich and Battisti [1991] studied the flow created by a steady point buoyancy source in a rotating stratified flow. *Helfrich* [1994] conducted a similar study of flow created by impulsive sources (called thermals). Scaling considerations were developed for velocity and length scales and successfully compared with laboratory experiments. An important result in both studies is that fluid would accumulate at a terminal depth until the heton mechanism produced eddy pairs that would remove the fluid.

The present study considers flow created by an extended but confined buoyancy source in rotating, stratified fluid. It can be considered to be an extension of *Maxworthy and Narimousa* [1991, 1994] with stratification added. Or, it can be considered to be an extension of *Helfrich and Battisti* [1991] with finite buoyancy size added. Laboratory experiments (in section 3) will test scalings (outlined in section 2).

Dynamical Considerations

Nondimensional Numbers

When an unstratified fluid of total depth H is forced to convect by uniform surface cooling in the presence of rotation f , there is only one nondimensional combination of the main external parameters B_0 , f , and H

$$R_0^* = \frac{\sqrt{B_0/f^3}}{H} = \frac{l_{\text{rot}}}{H}, \quad (4)$$

which will be called the natural Rossby number R_0^* (its physical significance is reviewed in *Marshall et al.*, [1994]). Here $l_{\text{rot}} = \sqrt{B_0/f^3}$ can be considered to be a measure of the vertical scale to which convection penetrates in an unstratified fluid during an inertial period. If R_0^* is large, then the convection will be limited by the ocean depth before it feels the effects of rotation; if R_0^* is small, then the convection will come under geostrophic control before encountering the bottom. Briefly, R_0^* is large in the atmosphere and small in the ocean. Only in oceanic regions which experience deep convection can R_0^* get small enough for rotation to be important. In the ocean, typical values for f , B_0 , and H are $f \approx 10^{-4} \text{ s}^{-1}$, $B_0 \approx 10^{-7} \text{ m}^2 \text{ s}^{-3}$ (corresponding to a heat loss of $\approx 2000 \text{ W m}^{-2}$), and $H \approx 1000\text{--}4000 \text{ m}$, giving an R_0^* in the range 0.08–0.4 so rotation cannot be neglected in the ocean. In the laboratory experiments presented

here R_0^* ranges from 0.04 to 0.41, and in our numerical experiments R_0^* varies from 0.05 to 0.58, both spanning the oceanic regime.

In addition to R_0^* , two additional nondimensional numbers are needed to fully describe the system when stratification and the size of a forcing region are included. The first is N/f , comparing the relative significance of stratification as measured by the frequency $N = [(-g/\rho) (\partial\rho/\partial z)]^{1/2}$ to rotation measured by f . The second is R_s/H , an aspect ratio comparing R , the radius of a circular forcing area, to the depth of the water column. In sites of deep ocean convection, N ranges from 2×10^{-4} to 10^{-3} s^{-1} ; thus N/f varies from 1 to 10. In the laboratory experiments presented here, $0.86 < N/f < 6.64$. They are thus in the lower limit of thermocline ocean values, making them particularly suited to deep ocean convection sites. Typical length scales for R_s are set by meteorological forcing and preconditioning dynamics and can range from a few to many hundreds of kilometers. The depth H varies from 1000 to 4000 m. This gives a range of $1.25 < R_s/H < 100$. In our experiments, R_s/H spanned 0.25–0.75. They are thus at the very lowest limit of real ocean values; nonhydrostatic effects may thus be exaggerated.

If viscosity and thermal conduction are of importance, the Taylor number $Ta = f^2 H^4 / \nu^2$ and Rayleigh number $Ra = B_0 H^4 / k^2 \nu$ may also be important. The critical value of Rayleigh number, which must be exceeded for convection to be important, has been related to the Taylor number [Chandrasekhar, 1953; Nakagawa and Frenzen, 1955] according to the relationship

$$Ra_f(cr) = kTa^{2/3},$$

where k is a constant dependent on the boundary conditions. *Bubnov and Senatorsky* [1988] determined k experimentally and found it to lie between 2.39 and 8.72, depending strongly on the boundary conditions used. In the laboratory it is impossible to achieve a value of H similar to that of the ocean. Using molecular values of ν and κ , typical laboratory values of Ra_f range from 10^{13} to 10^{15} , if f ranges from 0.01 to 0.1 s^{-1} , $H \approx 0.1 \text{ m}$, and $Ta \approx 10^5$, giving a critical Rayleigh number of $Ra_f(cr) \approx 10^6$. We thus exceed this critical value by several orders of magnitude. In the ocean $f \approx 10^{-4} \text{ s}^{-1}$, $H \approx 10^3 \text{ m}$, $\nu \approx 10^{-6} \text{ m}^2 \text{ s}^{-1}$, and $\kappa \approx 10^{-7} \text{ m}^2 \text{ s}^{-1}$ (for thermal diffusion in water), giving $Ra_f \approx 10^{27}$ and $Ta \approx 10^{22}$ vastly exceeding critical values.

Convection in a Stratified Rotating Ocean

Consider buoyancy forcing applied over a finite circular area only, so the parameters to be considered are B_0 , N , f , H , R , and time t . Previous work [Legg and Marshall, 1993; Jones and Marshall, 1993] has focused on the evolution of both individual and collections of convection cells. In the present study we concern ourselves with the development of the entire chimney which is

made up of many aggregates. Some parts of the subsequent discussion are due to *Visbeck et al.* [1996], where more details of the arguments may be found.

We consider first the vertical evolution of the mixed layer at a position in the center of the well-mixed chimney. For a sufficiently wide chimney a water parcel in this position will be unaware of any spatial inhomogeneity in either cooling or overturning. Before rotation becomes important, the evolution of the mixed layer can be described by a one-dimensional model. If there is no entrainment of fluid across the base of the chimney, then [see *Turner, 1973*],

$$h = \sqrt{\frac{2B_0 t}{N^2}} \quad (5)$$

As rotation becomes important, the chimney adjusts toward geostrophic balance. Simple analytical expressions are found in the work by *Gill et al.*, [1974] and *Crépon et al.* [1989]. From geostrophic adjustment theory we expect the wall of the chimney to have a width $R_d = Nh/f$, the Rossby radius of deformation. The surface convergence has an associated cyclonic velocity u_{rim} , which may be inferred from thermal wind thus

$$\frac{du}{dz} = \frac{g}{\rho f} \left(\frac{\partial \rho}{\partial r} \right), \quad (6)$$

implying

$$u_{rim} = \frac{gh}{\rho_0 f} \frac{\Delta \rho|_r}{R_D}, \quad (7)$$

where $\Delta \rho|_r$ is the density jump across the zone assumed to be of width R_D , r is the radius, and ρ_0 is a constant reference density.

We define the chimney geometry such that the density difference radially outward from the center is the same as the vertical density difference from the spreading level to the surface. Then by definition $(g\Delta \rho|_r/\rho_0) = (g\Delta \rho|_z/\rho_0) = N^2 h$. Hence, from (7)

$$u_{rim} = Nh, \quad (8)$$

since $R_d = (Nh/f)$. The rim current will continue to grow as h evolves in time until the onset of baroclinic instability. At that time eddies will form and begin to transport water (at a speed (7)) away from the chimney and also bring surrounding water in.

The instability timescale may be inferred from baroclinic instability theory [Eady, 1949]. The growth rate ω of the fastest growing mode in the rim current is

$$\omega \sim \frac{f}{\sqrt{R_i}}, \quad (9)$$

where $R_i = N^2 / (\partial u / \partial z)^2$ is the large-scale Richardson number. If the rim current is in thermal wind balance with speed Nh , then $R_i = 1$ and

$$\omega \sim f. \quad (10)$$

At this time, $t \sim f^{-1}$ our scales become

$$u_{\text{rim}} \sim \sqrt{B_0/f} = u_{\text{rot}} \tag{11}$$

$$R_d \sim l_{\text{rot}} \equiv \sqrt{B_0/f} , \tag{12}$$

and

$$h \sim \frac{f}{N} l_{\text{rot}} . \tag{13}$$

The above scales are interesting inasmuch as the instability timescale and the lengthscale of the preferred mode are seemingly independent of the stratification N . It is also fascinating to see the unstratified scales u_{rot} and l_{rot} appearing in this stratified problem; but see *Speer and Marshall* [1995] where they appear as key parameters in the hydrothermal plume problem also.

Equilibrium State

So the initial stages of the vertical evolution of the mixed layer are governed by the one-dimensional result, which is valid until baroclinic instability sets in on a timescale $t \sim f^{-1}$. At that time the baroclinic instability facilitates an exchange of fluid and properties between the chimney and the surrounding region. This lateral exchange inhibits the further vertical evolution of the mixed layer, so that the layer deepens less rapidly than the $t^{1/2}$ curve. Eventually, an equilibrium must be reached between the density forcing through the surface and the lateral removal of dense fluid by the baroclinic eddies, as detailed in the work of *Legg and Marshall* [1993]. This equilibrium necessarily halts further deepening of the mixed layer; the depth at this time will be the maximum depth achieved and may be derived as follows. The balance between the buoyancy flux through the surface and the lateral transport is [*Visbeck, et al.*, 1996]

$$\int \frac{B_0}{g} dA = \frac{1}{\rho_0} \int \oint \overline{v'\rho'} dldz , \tag{14}$$

where v is the horizontal cross-stream velocity, the prime denotes deviation from the average, and the bar denotes a time average. From energy analysis of the baroclinic region we can write [*Eady*, 1949; *Green*, 1970; see also *Visbeck, et al.*, 1996]

$$\overline{v'\rho'} = \frac{g}{N\rho_0} \overline{\rho'^2} , \tag{15}$$

where ρ' is the perturbation density anomaly achieved when moving a water parcel in the baroclinic region. Since (as discussed above)

$$\frac{g\rho'}{\rho_0} \sim N^2 h , \tag{16}$$

$\overline{v'\rho'}$ scales as

$$\overline{v'\rho'} \sim \frac{\rho_0}{g} N^3 h^2 . \tag{17}$$

Then the equilibrium balance (14) becomes

$$\frac{1}{g} B_0 \pi R_s^2 \sim \frac{1}{g} 2\pi R_s N^3 h^3 , \tag{18}$$

which reduces to

$$h \sim d_s = \frac{(B_0 R_s)^{1/3}}{N} . \tag{19}$$

The quantity d_s is the scaling for the maximum depth achieved by the convective mixed layer, assuming all available potential energy is converted to eddy kinetic energy by baroclinic instability. The result (19) is derived in more detail in the work of *Visbeck, et al.* [1996]. This scaling for penetration depth has no f dependence.

Now let us investigate the scales of the baroclinic instability in the context of the evolution of the mixed layer. We know from the solution of *Eady's* [1949] baroclinic instability problem that

$$l_{\text{eddy}} \sim R_D \sim \frac{Nh}{f} = l_s . \tag{20}$$

As h increases, then so must l_s in accordance with the expressions derived above for h . The number of eddies present is dependent on the integral number of wavelengths that may be contained about the circumference of the chimney, that is,

$$M \sim \frac{2\pi R_s}{l_s} \tag{21}$$

Again, this number will change with time as l_{eddy} grows. This prediction is borne out by the data presented below; initially, h is small, and the chimney begins to break up into eddies. As time goes on, h increases, and one sees the eddies coalesce. Ultimately, the number of eddies actually shed is smaller than the number of waves initially visible at the onset of instability. At the equilibrium depth we expect, setting $h = d_s$,

$$M_s = \frac{R_s^{2/3} f}{B_0^{1/3}} .$$

To summarize, we now have scalings for the velocity of the rim current in the baroclinic zone, the number of baroclinic eddies formed, their associated length scale, and the equilibrium depth of the convectively produced dense water. These scaling predictions are henceforth denoted by the additional subscript s

$$u_s = N d_s = (B_0 R_s)^{1/3} \tag{22}$$

$$l_s = \frac{N d_s}{f} = \frac{(B_0 R_s)^{1/3}}{f} \tag{23}$$

$$M_s = \frac{R_s^{2/3} f}{B_0^{1/3}} \tag{24}$$

$$d_s = \frac{(R_s B_0)^{1/3}}{N} . \tag{25}$$

Note that the first three above are independent of N , and the last one is independent of f .

Finally, it is interesting to consider the final volume of dense water produced during a convection event. An upper limit is given by the fastest rate at which dense

water may be produced. The shortest time in which the system can reach d_s is given by the time it would take the one-dimensional model to evolve to d_s . Once the one-dimensional model ceases to be valid, vertical evolution is slowed under the stiffness imposed by rotation. So the shortest time required by the system to reach d_s is given by equating h in (5) with d_s in (25) which gives the timescale

$$t_s = \left(\frac{R_s^2}{B_0} \right)^{1/3}. \quad (26)$$

Then the rate Q at which dense water is produced scales as the volume of the cylinder beneath the source divided by t_s so

$$Q \sim Q_s = \frac{R_s^2 d_s B_0^{1/3}}{R_s^{2/3}} = \frac{R_s^{5/3} B_0^{2/3}}{N} \quad (27)$$

Many of the above scalings, but particularly (22)–(25), will now be tested against the laboratory results.

Laboratory Observations of Deep Water Convection in Rotating Stratified Fluid

Although many theories have been developed and observations taken of rotating convection, little is known about the convective overturning of a rotating stratified fluid. Here attempts have been made to systematically develop experiments and techniques to investigate convection in stratified fluid. We are particularly interested in convection which is produced by the addition of density over a limited surface area since it has obvious implications for the ocean.

Density Increase by Spraying

The first laboratory experiment was exploratory in nature, although some quantitative information about eddy size and velocity magnitudes was obtained. The apparatus (Figure 1) consists of a linearly stratified rotating fluid produced by the Oster method in a square glass rotating tank $113 \times 114 \text{ cm}^2$ which is 50 cm deep. In the Oster method the tank is filled using two identical cylindrical source tanks, one with fresh water and the other with salty water. Both have free surfaces exposed to the air. Water from the fresh tank is slowly introduced to the rotating tank through a rotating connection and into a bed of fine stones on the bottom of the tank. Meanwhile, water from the salty tank is fed into, and mixed within the freshwater tank, so that the levels of the two tanks slowly decrease together. The density of the introduced water increases linearly with time, and each element of water injected spins up in the stone bed so that the net effect is a rotating stratified body of water. Stratification in a tank filled carefully by this method can be relatively constant; Figure 2 shows density versus depth at the start of a typical exper-

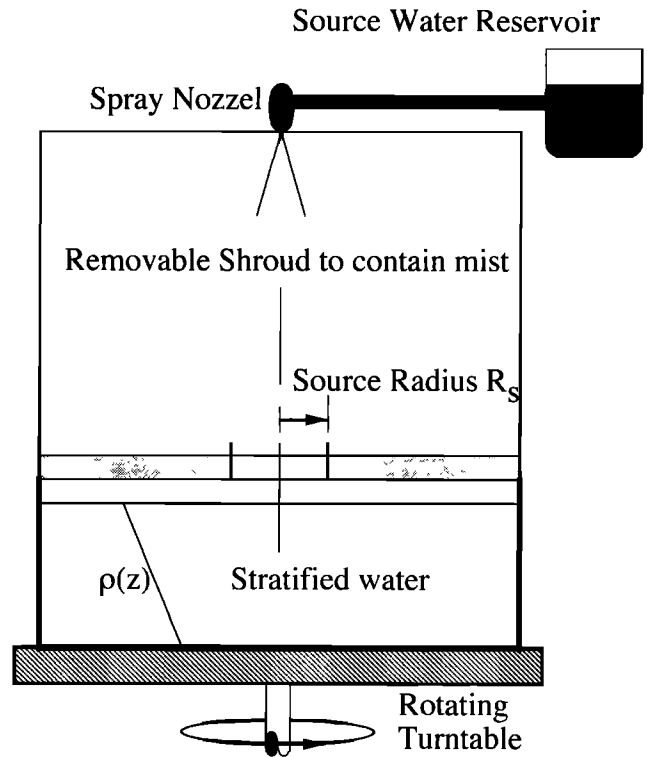


Figure 1. Sketch of the apparatus for producing a buoyancy flux with a paint sprayer onto the surface of a rotating stratified fluid.

iment. Lateral circulation of water in the tank from small uneven filling is quite small and is measured from the drift of columns of potassium permanganate to be less than 0.1 mm s^{-1} .

To generate convection, the addition of salty water at the surface was preferred to surface cooling. For 60 s a fine mist of almost completely salt-saturated

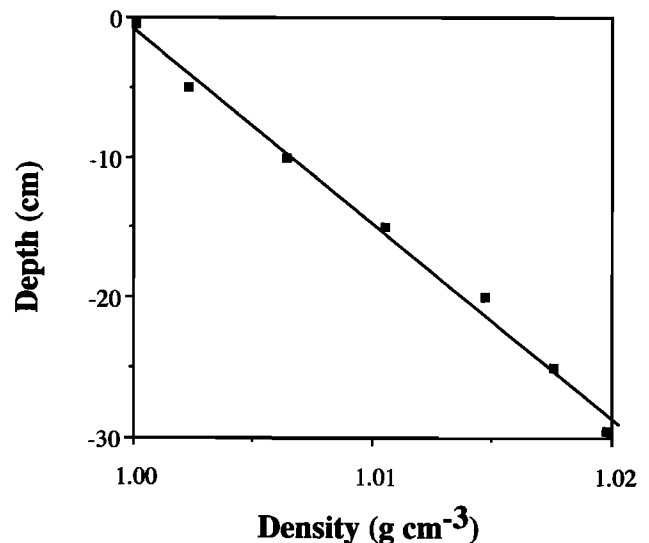


Figure 2. A typical distribution of density with depth in the test tank after it is filled by the Oster method.

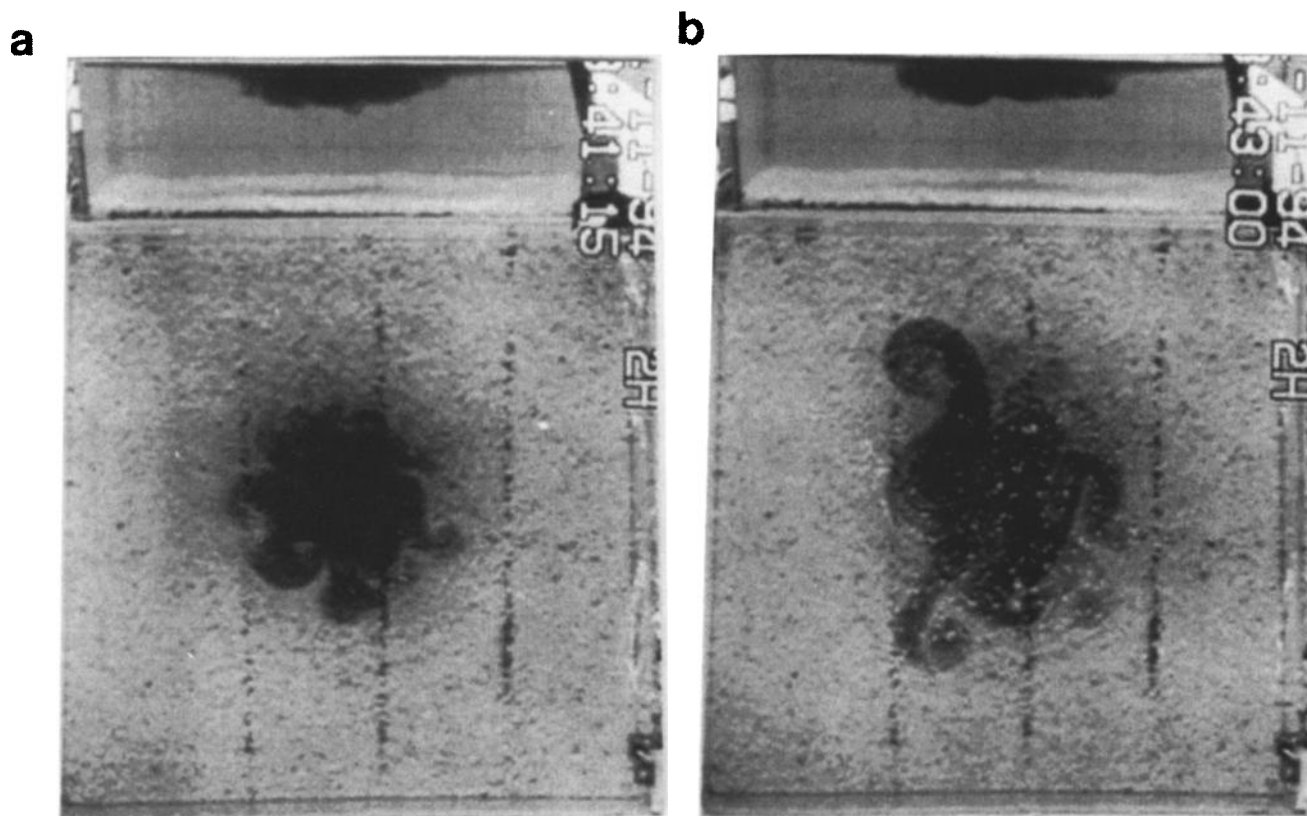


Figure 3. Views of eddies produced in experiments with the paint sprayer forcing after the shroud has been removed at (a) 75 s after start and (b) 180 s after start. The top parts of the figures contain a side view of the water through a 45° mirror. The bottom parts show the top view of the water. In this experimental run, $f = 0.5 \text{ s}^{-1}$, $N = 0.43 \text{ s}^{-1}$, and $B_0 = 0.32 \text{ cm}^2 \text{ s}^{-3}$.

blue food coloring (ρ close to 1.2 g cm^{-3}) is sprayed onto the top surface of the stratified water that was 30 cm deep through a 30-cm-diameter hole. The mist was produced by a paint sprayer, which was located about 120 cm above the tank. The sprayer was enclosed in a lightweight shroud to prevent salt spray from contaminating the laboratory equipment. The sprayer and shroud were quickly removed after 60 s of spraying. The total volume of salt-saturated solution introduced through the hole was measured to be 61 cm^3 to within 10% error, giving a buoyancy flux $B_0 = g\Delta\rho V/\pi r^2 t$ of roughly $0.3 \text{ cm}^2 \text{ s}^{-3}$. This produced greater values of buoyancy fluxes than could be obtained from surface cooling. For comparison the buoyancy flux $g\alpha H_f/\pi r^2 \rho c_p$ from $H_f = 500\text{-W}$ cooling over the same area is about $0.03 \text{ cm}^2 \text{ s}^{-3}$. (For this calculation we used a specific heat of $4.1 \text{ J g}^{-1} \text{ m}^{-1} \text{ }^\circ\text{C}^{-1}$, density = 1 g cm^{-3} , $g = 980 \text{ cm s}^{-2}$, and $\alpha = 2 \times 10^{-4} \text{ }^\circ\text{C}^{-1}$.)

Two cameras rotating with the turntable produced video images of the movement of the dyed fluid and of pellets scattered on the top surface. The experiment was recorded on videotape for at least 15 min after the sprayer was turned off. A color camera obtained a top view together with a side view through a 45° mirror. The top view was only obtained after the spraying had

finished and the shroud was removed. The side view in the mirror was visible for the duration of the run. A second, black and white camera recorded a close-up of the side view in order to record the advance of the mixed layer. The depth of the dyed mixed layer was occasionally recorded by eye with a meter stick during the experiment for additional calibration.

As time progressed, the mixed layer advanced downward during the first 60 s and stopped advancing when the spray was turned off. After the shroud was removed, it was clear that the patch of dense dyed fluid had, more often than not, broken into a number of eddies as shown in Figure 3. These eddies were correlated with cyclonic surface circulation. However, as the eddy field slowly broke up, a deeper patch of dyed fluid was invariably seen to lie to the right (looking radially outward from the center of the density source) of each cyclonic eddy. We now recognize such eddy pairs as a common laboratory example of the heton arrangement [Helfrich and Battisti, 1991], in which the anticyclonic component of the circulation within such a heton is concentrated at depth rather than at the surface. Photographs from four runs are shown in Figure 4. The variation in eddy sizes and depth of penetration is obvious. Each row has the same value of f with the top row being larger by a factor of 4. Each column has the same value of N with

the left column being larger by a factor of about 4. The correlation of eddy size with row and depth of penetration with N is clear. These are the end-members of nine such runs which showed an unmistakable relationship of eddy size with f and depth with N . Selection of values of buoyancy flux B_0 , fluid depth H , stratification N , and rotation rate f depended on the following factors:

1. For a set of experiments in which R_s , N , and f are systematically varied, B_0 is set at the maximum value we can produce. This ensures that convection cells are as vigorous as possible. The present value of B_0 ranged from 0.17 to 0.3 cm² s⁻³ in most of the runs. This produced values of l_{rot} between 1 and 13 cm so that rotational effects were experienced within distances less than the depth of the tank. The use of larger rather than smaller values of B_0 avoids a problem that arises in thermal cooling experiments, in which cooling is limited by heat flux through the top and which typically lead to B_0 values which are an order of magnitude smaller than used here. If as is typical, rotation rates in the range $0.1 > f > 1.0$ s⁻¹ are used in such experiments, values of l_{rot} are so small that molecular processes become important. The only way to remove this problem in thermal experiments is to use smaller values of f . However, these experiments require smaller values of N if the deformation radius is to be small enough to allow baroclinic instability – (see comment 3 below). This low stratification invariably produces very shallow mixed layers with baroclinic eddies limited to the top centimeter or two near the surface. It is thus difficult to observe. Moreover, the Rayleigh number of this shallow layer is small. The present experiment, with its supporting scaling arguments and larger values of B_0 , overcomes these shortcomings.

2. Although the largest possible value of B_0 is desirable, only a small amount of saturated salt solution should be added to increase the density of the mixed layer. Given the salinity of saturated salt solution this fact not only limits buoyancy flux but also was found to limit $N < 1.0$ s⁻¹, since for greater values of B_0 the mixed layer penetrated to the bottom of the tank.

3. It was also necessary to ensure that the baroclinic eddy size be of the order of or less than the radius of the source. More importantly, no experiments were conducted in which the eddies reached the outer wall during the run. The eddy-size constraint dictates roughly that $Nd/f < 40$ cm. With N equal to its greatest value of ~ 1.0 s⁻¹ and d of ~ 10 cm this implies, roughly, $f > 0.25$ s⁻¹. In our experiments, runs with $f = 0.125$ gave the largest permissible eddies, and since eddy size was found to be inversely proportional to f , smaller values were not used. Indeed, smaller values would result in the eddies reaching the outer wall of the tank before the mixed layer had reached its maximum depth.

4. It was important to try and conduct the experiments in the range with $N/f = 1$ or greater, the predominant range of interest in the ocean.

5. The centrifugal acceleration had to be limited to a small fraction of gravity so that the surface of the fluid remained almost perfectly flat. This prohibits use of values of $f > 0.5$ s⁻¹.

The above considerations resulted in the following experimental parameter ranges: $0.2 < N < 0.9$ s⁻¹, $0.125 < f < 0.5$, s⁻¹, and $0.17 < B_0 < 0.3$ cm² s⁻³. Since the scaling laws predict low sensitivity to B_0 , some additional runs were conducted by varying B_0 through 2 orders of magnitude (with N being appropriately adjusted to result in the same penetration depth). In these runs, N/f was mostly less than 1 and so not in the optimal parameter space.

Measurements taken and associated errors.

Estimates of eddy size were made by measuring the diameter of every clearly visible cyclonic eddy recorded on the video after the patch of densified fluid had spread out sufficiently to clearly identify each eddy. Speeds were found by measuring the distance that small paper discs moved in 3 or 4 s. These measurements were taken during the same time interval as those of radial distance. The depth of the mixed layer was identified as the bottom of the dyed layer, and measurements of this depth were taken directly by eye as the experiment progressed (d_e), from the side view tape (d_{sv}), and from the top view through the mirror (d_m).

Error in the velocity measurements is difficult to define since the most rapid velocity of the surface pellets was selected for measurement. The actual measurement of the position of the particle and the time is very precise (to a couple of millimeters and to 0.03 s, respectively), but there is no way to guarantee that this is the true peak velocity in the entire velocity field. We suspect there is no other velocity twice as great as the values we report, for instance, but the span shown is as good as can be obtained with our present facility.

Error for size and wavenumber of the eddies depends as much on identification of the eddies as on experimental precision. The dye technique appears to allow every eddy to be filled with dye. In observing the eddies in real time or by viewing the videotape, we found no evidence that eddies without dye were present. It is important to keep in mind that the eddies and currents generate their own mesoscale variability.

Error in measurement of convective depth from the side view camera was estimated to be about 2 cm for the most extreme cases. This error was mostly from uncertainty of parallax corrections, since the side view contained no information about whether a particular deeply penetrating blob lay close to the camera or further away. Error in the measured depth from the video camera that showed both a top view and the side view mirror was limited by resolution of the video camera. Each individual video line resolved about 0.5 cm, but the estimate of depth could be off by a total of four or five lines depending on lighting, lumps in the penetrating eddies, and other visual interpretation aspects.

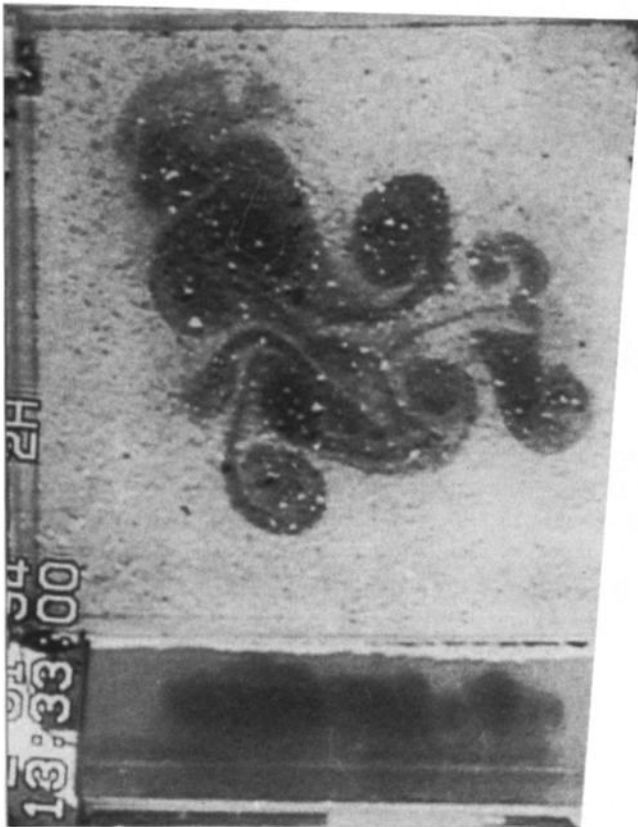
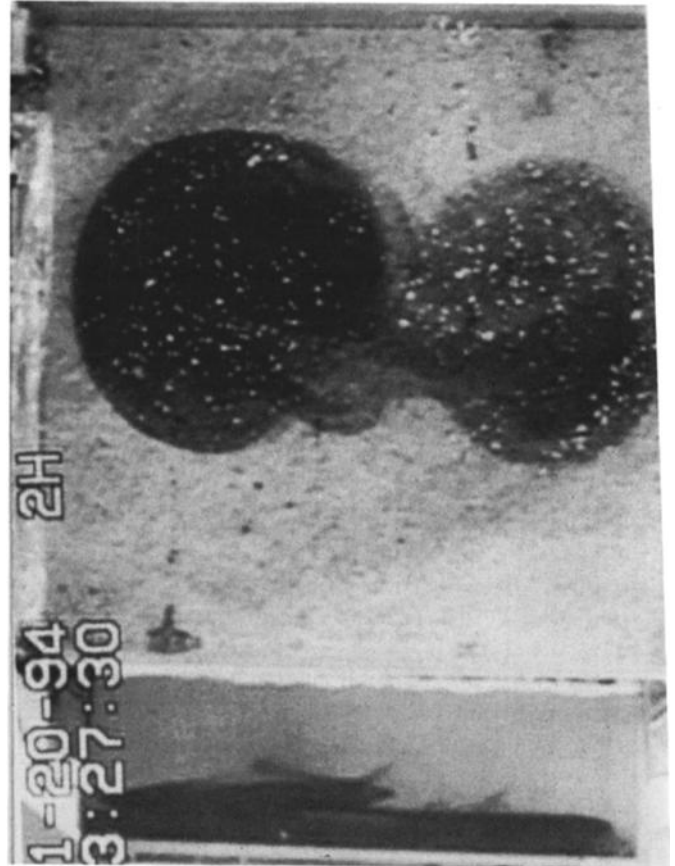
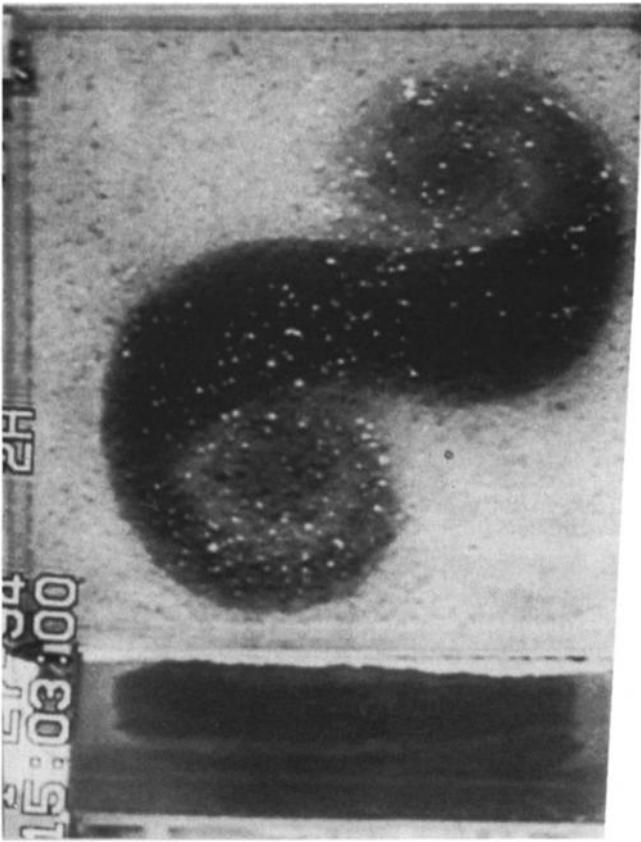


Table 1. Results From the Spraying Experiments With $R_s = 15$ cm.

f (s^{-1})	N (s^{-1})	B_0 ($cm^2 s^{-3}$)	d_e (cm)	d_{sv} (cm)	d_m (cm)	Eddy Size (cm)	Velocity ($cm s^{-1}$)
0.250	0.83	0.29	-	-	7.5	12,18,20	1.0-1.2
0.250	0.41	0.27	-	12	12.5	16,16,18	0.94-1.5
0.250	0.22	0.27	-	>25	<i>b</i>	20,20,21	0.8-1.5
0.125	0.83	0.29	-	-	10.2	27,28	1.2-2.1
0.125	0.41	0.27	12	12	14.3	32	1.5-1.6
0.125	0.24	0.29	-	25	<i>b</i>	27,32	1.6-2.1
0.500	0.82	0.29	6	-	7.5	7,8,8,8,9	0.47-0.9
0.500	0.45	0.28	-	12	11.6	6,7,8,8,9	0.6-0.8
0.500	0.20	0.28	-	25	22.5	7,7,8,8,8	0.6-1.3

Thus the error of the two cameras is comparable. Depth measurements ranged from 4 to 27 cm, but depth errors do not range from plus or minus 8 to 50%, since the small depths exhibited smaller uncertainties in parallax and variation in individual blobs. Thus a more realistic range of uncertainties is from plus or minus 8 to 30%.

It should be emphasized, however, that the biggest source of scatter in the data is due to natural variability associated with eddies. This scatter is visible in the ranges shown in the tables and figures and is not a consequence of measurement error. The scatter could only be reduced significantly by a much greater statistical study, which is prohibitively expensive, rather than by improvement of measurement technique.

Paint sprayer results. After some preliminary runs, nine experiments were conducted with this paint sprayer arrangement. The results of these measurements are shown in Table 1 and in Figures 5 and 6. In two cases the dye was close to the bottom. The letter *b* denotes this in Table 1.

Equations (12) and (23) for l_{rot} and l_s predict that the size of the eddies is sensitive to rotation but not to stratification. This is borne out by the data shown in Figures 5a and 5b where the eddy size for five experiments is plotted against the Coriolis parameter. It is clear that the data are not only relatively insensitive to N but that they follow a trend like the inverse of f . In Figure 5a the data on eddy size exhibit clear sensitivity with f to within a few percent. The average eddy sizes and standard deviation for the three progressively greater values of f are (in centimeters) 28.2 ± 3.4 , 16.9 ± 2.2 , and 7.7 ± 0.7 , respectively. The standard deviations are 13% or less of the mean values, yet N varies by a factor of 4. In Figure 5b the data on eddy size are

shown with logarithmic axes. The least squares log-log regression formula is shown, and the exponent of -0.97 is very close to -1 . In Figure 5c the sensitivity to variation of N is shown. There is little variation with N compared to the sensitivity to f . The sensitivity to N is clearly very weak. The data for eddy size are plotted against $(B_0 R_s)^{1/3}/f$ suggested by (23) in Figure 5d. The regression line has a slope of 2.3 and a correlation coefficient of 0.96. All the experiments in Table 1 had roughly the same value of B_0 and so should have the same velocities according to (22). The nine values of maximum velocity were averaged and then divided by the average value of $(B_0 R_s)^{1/3}$. The result was 0.9. Data for mode number were taken as the number of eddies in Table 1. That number plotted against the formula $R_s^{2/3} f/B_0^{1/3}$, as suggested by (24), gives a line of slope 0.95 with a correlation coefficient of 0.98. The lengths and velocities divided by their scales are also shown plotted against the two dimensionless numbers N/f and R_0^* in Figure 6. Although there is scatter, there is only weak dependence on these dimensionless numbers. Moreover, the coefficients are in the range of 0.9 for velocity and 2.3 for length scale.

Experiments With Steady Buoyancy Flux

Although the paint sprayer method had the advantage of producing an unobstructed plan view of the eddies, its most serious limitation was that the sprayer had to be stopped to enable the convection to be observed. This means that, unfortunately, there is no guarantee that paint-sprayer velocities, eddy sizes, or penetration depth lie at their final values. The second set of laboratory experiments was designed to overcome this problem. To generate a buoyancy flux at the top

Figure 4. Four photographs (directly from videotape) of dyed fluid after the paint sprayer is removed. Each was taken downward from above the rotating tank. In the top of each photograph is a side view through an angled mirror. The two top photos have a value of $f = 0.5 s^{-1}$ and two bottom have a value of $f = 0.125 s^{-1}$. The left column has N of about $0.8 s^{-1}$, whereas the right has N of about $0.2 s^{-1}$.

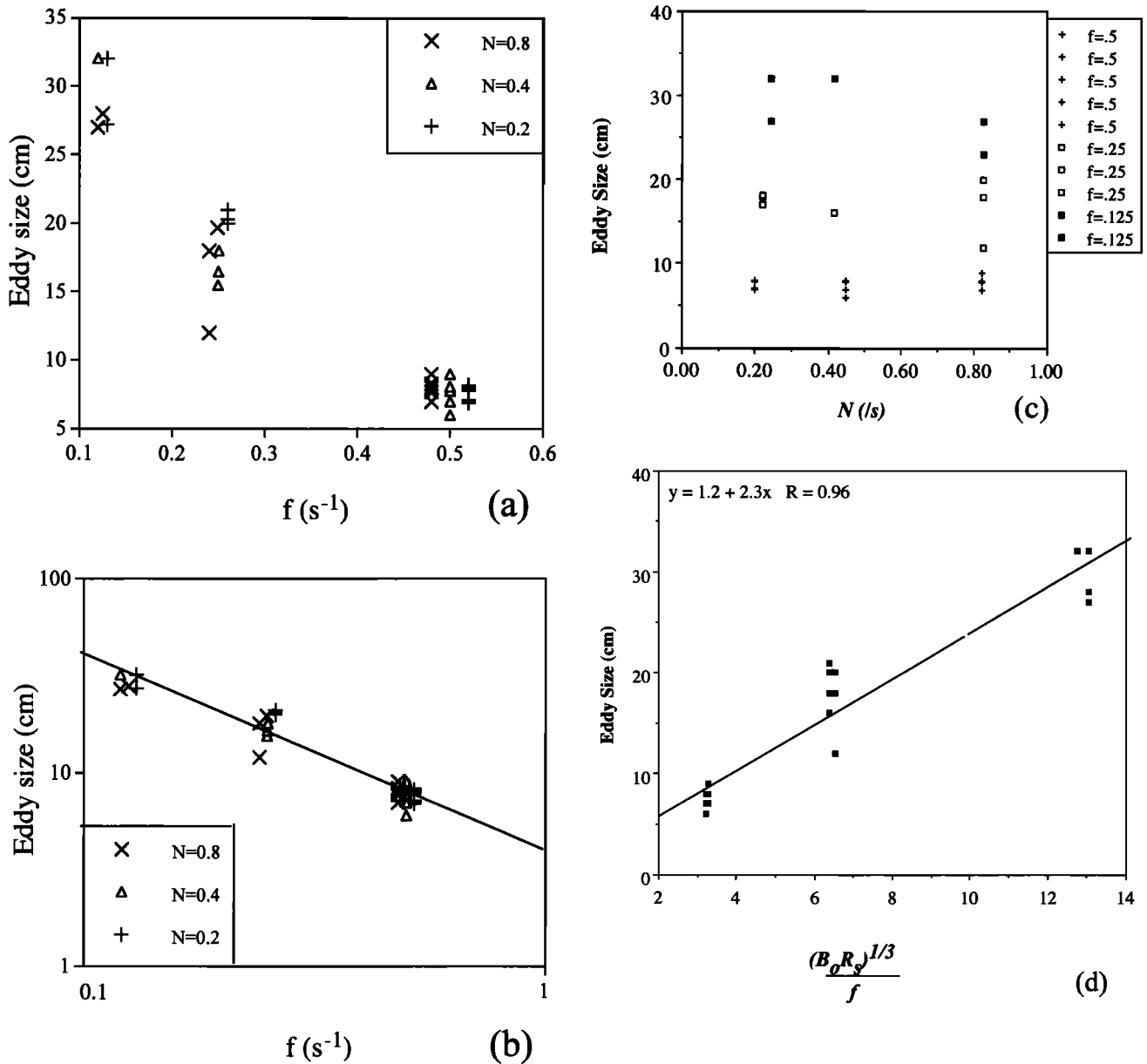


Figure 5. a) Eddy size as a function of Coriolis parameter f for assorted values of N . b) Same as in (5a) but on log-log coordinates. A least squares fit line and formula are given. The slope is very close to -1 . (c) Eddy size as a function of stratification N . d) Eddy size as a function of $(B_0R_s)^{1/3}/f$. A least squares fit line and formula are shown.

surface, a cylinder of either 15-, 30-, or the 45-cm diameter with Whitman filter paper attached to the bottom was placed in contact with the free surface of the water (Figure 7). Although this had the limitation that the overhead view of the experiment was partially obscured, the buoyancy flux could be continued indefinitely, allowing the depth of penetration to be monitored over a long period of time. As in the first experiment, the ambient fluid consisted of a linearly stratified rotating fluid produced by the Oster method in the same glass tank ($113 \times 114 \text{ cm}^2$). The porosity of the filter paper was selected so that the flux through the filter paper

was of the desired rate if the standing water depth in the cylinder was 2 or 3 cm. This ensured that the flow into the tank was spatially uniform.

In practice, two values of porosity were employed. In the 15-cm-diameter cylinder, Whitman 5 paper was used, since it was readily available from the stockroom. To start the experiment, the fluid depth in the cylinder was brought to 1.7 cm by manually pouring in 300 cm^3 of brine. A pump was immediately started and supplied fluid at a volume flux of $Q = 0.25 \text{ m}^3 \text{ s}^{-1}$. This was the rate that water was estimated to seep through the paper from the supplier's specifications of porosity

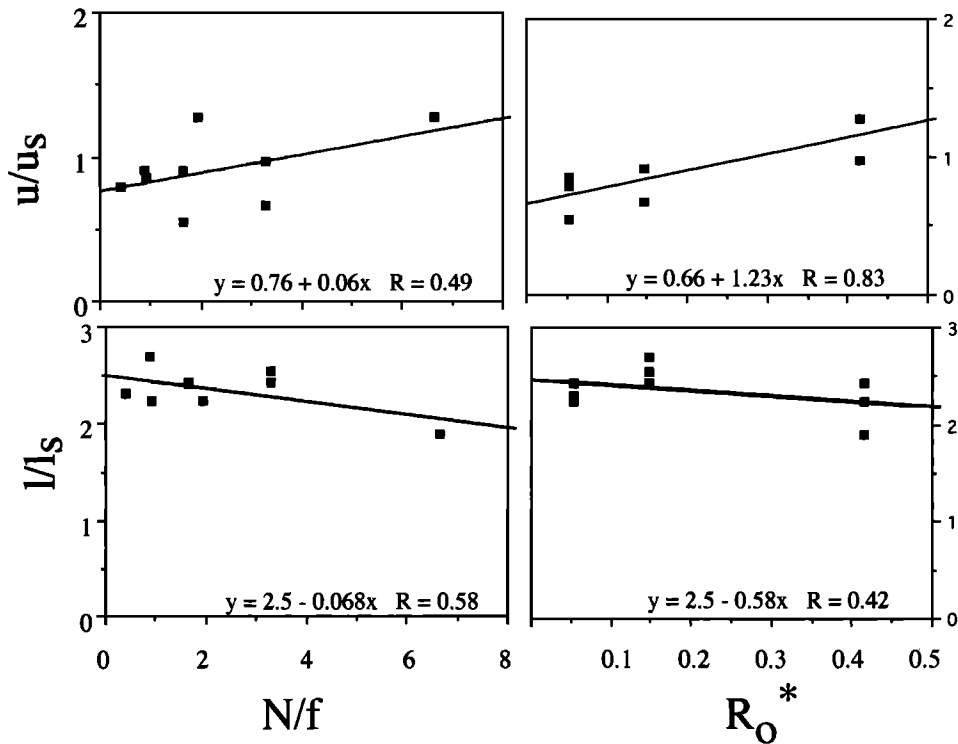


Figure 6. Velocity and size of eddies divided by their scales as a function of 2 dimensionless numbers that varied in the runs shown in Table 1. Least squares fits to the data are also shown along with their formulae and regression coefficient.

with a 1.7-cm head. In this manner a constant depth of fluid in the cylinder was maintained. This depth was measured periodically and found to remain to within 0.1 cm of the desired depth. Thus the flow of brine into the stratified tank is estimated to produce a buoyancy flux $B_0 = Qg\Delta\rho/15^2\pi = 0.28 \text{ cm}^2 \text{ s}^{-3}$. Paper of different porosity, Whitman 542, was used for the larger-diameter experiments, 30 and 45 cm. This produced values of $B_0 = 0.17$ and $0.3 \text{ cm}^2 \text{ s}^{-3}$ for standing depths in the cylinder of 1.7 and 3 cm, respectively. Smaller depths were used for some experiments, since larger heads produced significant sag of the paper in these larger cylinders.

In all experiments the procedure was the same. A fixed volume of brine dyed with blue food coloring was added to the cylinder. A pump was then activated to supply identical fluid continuously at the rate of volume flux estimated to flow through the filter paper. The depth of fluid above the filter paper was monitored and observed to vary by less than 30% for the duration of the experiment of either 15 or 20 min. By varying the salinity of the fluid in the cylinder, buoyancy fluxes could be achieved equal to that of the paint sprayer of $0.3 \text{ cm}^2 \text{ s}^{-3}$, down to a value 100 times smaller.

As before, two cameras rotating with the turntable recorded the movement of the dyed fluid and of pellets scattered on the top surface. The data were recorded on videotape for a duration of about 20 min. The camera recording the side view was set so that the depth of

penetration could be measured as accurately as possible, to within some 2 cm. The depth of the dyed mixed layer was occasionally recorded by eye with a meter stick during the experiment. The greatest uncertainty is from parallax, since some of the fluid is closer to the camera and other fluid is further away. A color camera was used to obtain a top view plus a side view through a 45° mirror. The cylinder obscured the central area in the top view, so only intrusive fluid that spread laterally could be seen from above. The side view in the mirror was visible for the entire duration of the experiment.

As time progressed, the mixed layer advanced downward. The principal measurement was of the depth of the dye. The time for the dye to reach each centime-

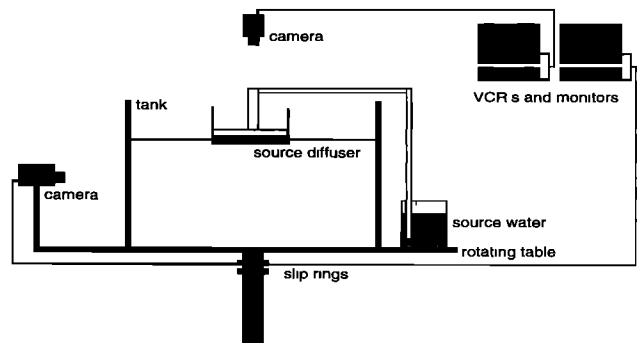


Figure 7. Sketch of the apparatus for producing convection continuously with time.

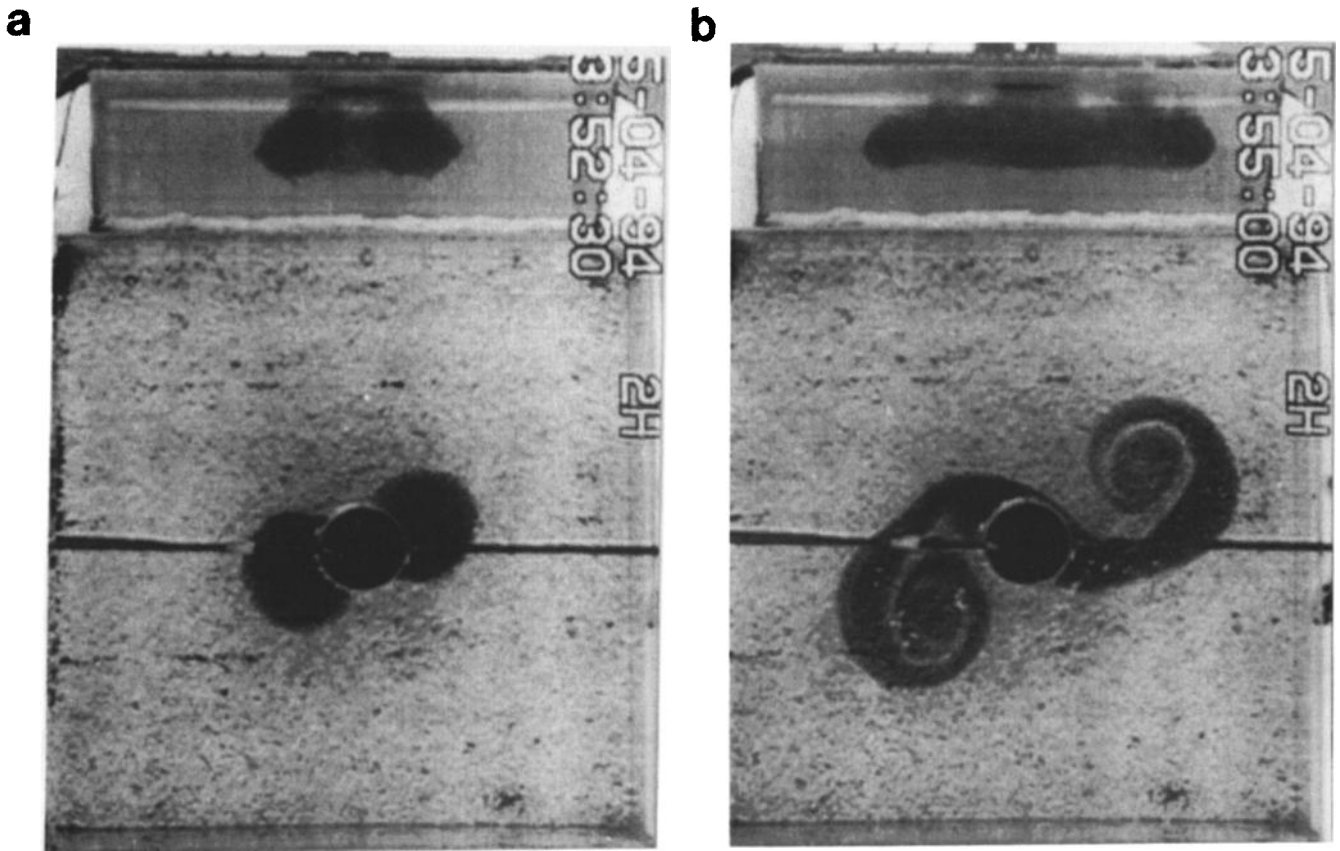


Figure 8. Views of eddies produced in experiments with continuous forcing. The tops of the panels contain a side view of the water through a 45° mirror. The bottoms of the panels show the top view of the apparatus. a) After 150 s with $f = 0.25 \text{ s}^{-1}$, $N = 0.22 \text{ s}^{-1}$, and $B_0 = 0.32 \text{ cm}^2/\text{s}^3$, the downward intruding water is splitting. The radius of the source is 7.5 cm, and the Rossby radius l_s is 5.4 cm. (b) After 300 s, two eddy pairs are well formed and are conveying the fluid away from the center. The two surface eddies are cyclonic and clearly indicated by the circular spirals that go counterclockwise inward. The two deeper eddies are not very visible in this picture, but they are located roughly under the arms extending from the spirals to the center of the tank. c) An experiment with a larger source radius of 22.5 cm after 150 s with $f = 0.5 \text{ s}^{-1}$, $N = 0.43 \text{ s}^{-1}$, and $B_0 = 0.17 \text{ cm}^2/\text{s}^3$. A number of waves are seen around the rim of the intruding water. The Rossby radius is smaller ($l_s = 3.1 \text{ cm}$) than for Figure 8a and Figure 8b. (d) After 360 s a number of eddies transport the dense water sideways.

ter depth level was taken visually from the videotape. The depth levels were calibrated by an image of a vertical meter stick that was placed in the middle of the tank, then moved to a number of locations closer and further away from the camera. This calibration was also checked against other geometrical features such as a background grid and calibration tapes on the tank edges. A correction was also made for bulging of the filter paper from the hydrostatic load of the dyed fluid. This was a little over a centimeter in the experiments with the 45-cm-diameter source and less for the smaller source. This sag was visible through the side view mirror and was directly subtracted from depth data. The estimate of plus or minus 2 cm includes this correction.

As in the experiments driven by the paint sprayer, the mixed layer penetrated rapidly downward in the early part of the run. Its rate of advance slowed noticeably after a time which was relatively easy to discriminate but generally never ceased for the duration of a run. Usu-

ally when the advance slowed, the side view revealed considerable lateral slumping of the sides of the dyed region, but unstable eddies had not yet developed. As time progressed, however, the patch of dense dyed fluid broke into a number of eddies as observed in the earlier experiments. The mixed layer depth at the longest permissible time was recorded as the final depth in Table 2. This longest time was either the duration of the recording or the time when an eddy hit the sidewalls of the tank.

Some aspects of the circulation are revealed in top and side photographs displayed in Figure 8. The dye would typically collect under the source as a rapidly deepening mixed region for early times. At some stage, waves would appear around the rim of the dyed fluid. The dye would quickly accumulate at lobes which were offset by a cyclonic surface circulation. The lobes would pair with such cyclones and propagate away from the source region.

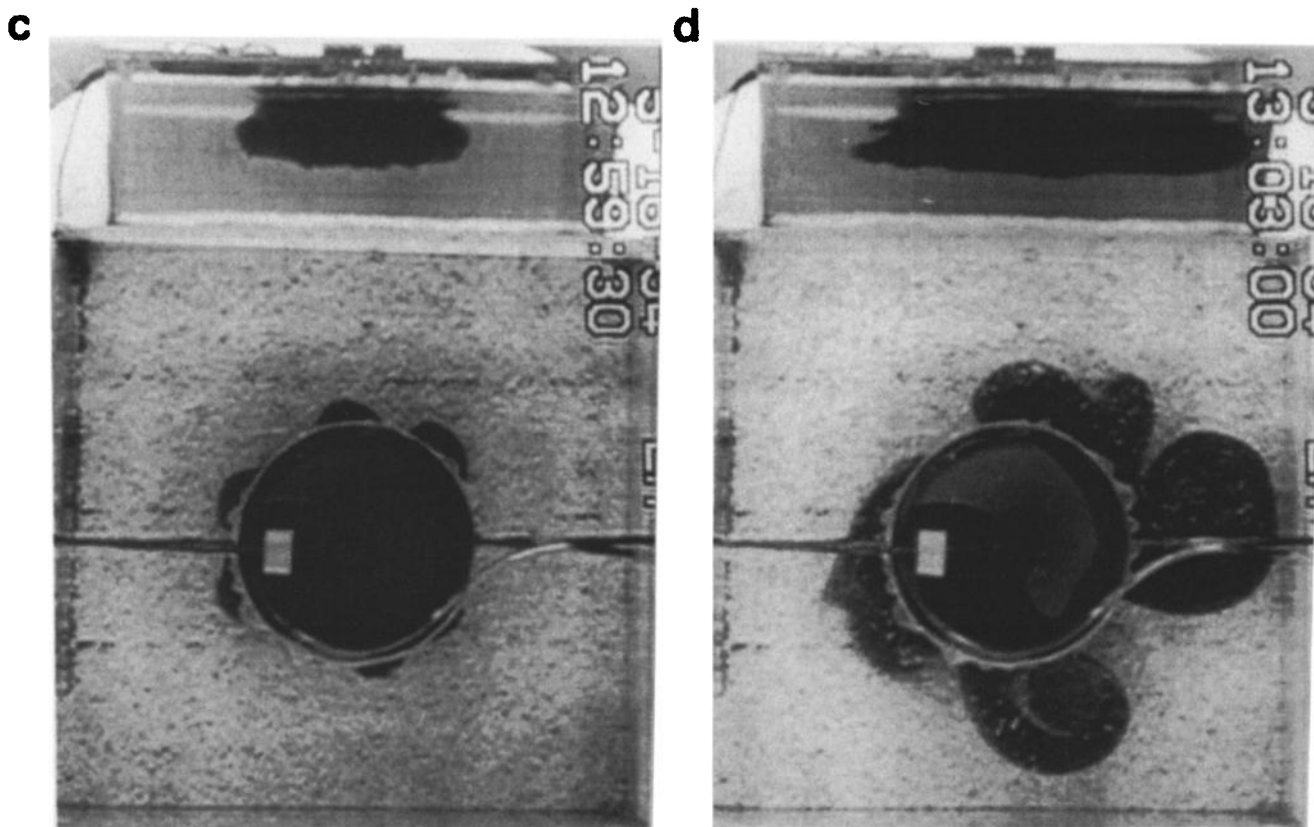


Figure 8. (continued)

Our theory for the final depth suggests that there is no dependence on f . This is well borne out by the data shown in Figure 9a, where the progression of the depth with time is shown for a number of runs with roughly the same value of N (about 0.4 s^{-1}). Values of f range over a factor of 4. Despite a fourfold variation in f , the depth for large time ranges between 15 and 20 cm or about 30%, less than one tenth the variation in f . For experiments in which N varied by almost a factor of 4, there is a lot of sensitivity, however, as shown in Figure 9b. The depth varies with N by about a factor of 4. The scatter in Figure 9a of about 0.3 and the scatter in Figure 9b of about 4 differ by more than a factor of 10. This is significantly greater than any possible measurement error or scatter from mesoscale variability. Within the range that is thought to apply to the theory, for $N/f > 1$ and $R_0^* < 0.6$, the final depth of the convection as a function of the predicted depth $d_p = (B_0 R)^{1/3}/N$ seems to cluster about a linear regression line (Figure 10). Data from experiments whose parameters span a factor of 5800 are shown in the Figure 10. The squares represent the data judged to be in the most relevant parameter space and these have a range of 4 in f , 2.6 in N , and 3 in R_s for a total range of 31. The data show reasonably good scatter about the least squares fit line with a regression coefficient of 0.81. The constant of proportionality between h and d_s in (19) is 4.6.

A final test of the theory was made from the prediction that depth should be proportional to $B_0^{1/3}/N$. To

test this, five runs were conducted (July 14–21), where B_0 was varied over a range of 2 orders of magnitude. This was accomplished by varying both the salinity of the injected fluid and the value of N to keep the ratio $B_0^{1/3}/N$ constant. Figure 11 shows the depth of the dye versus time for the five runs. The depth is clearly approaching ~ 16 cm for most cases. Three trajectories track one another fairly closely. They correspond to the three data points that lie in the upper left in Figure 10 and may correspond to a dynamic balance (not necessarily covered in our scaling discussion) valid for small N/f . The trajectory for the run denoted by crosses had the largest value of N/f , and it actually agrees most closely with the data shown by solid squares in Figure 10. With such a small number of runs one cannot be definitive about the value of the exponents of the various terms, but the following estimate is useful: Averaging all five final depths from Table 2, we obtain 13 cm with a standard deviation of 2.1 cm, 16% of the average value. If this deviation is due entirely to scatter of n in the formula B^n/N , then the range of n around $1/3$ is estimated as $\ln 1.16/\ln 10 = 0.06$, suggesting that $0.27 > n < 0.39$.

Discussion

The laboratory experiments clearly show that the downward advance of the mixed layer ceases after a given time. Then dense water formed by the surface buoyancy flux spreads laterally within baroclinic eddies

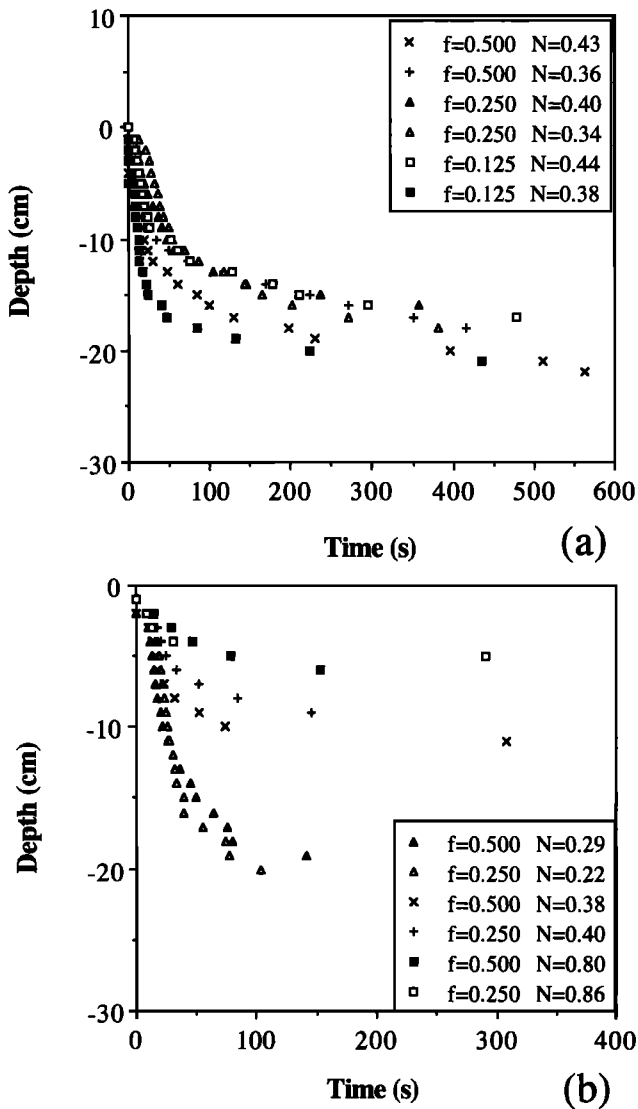


Figure 9. a) The advance of depth of the mixed layer with time for runs with similar values of N , 2 values of R_s , and more strongly varied values of f . The plot illustrates the relative insensitivity of depth with f and to a lesser extent with R_s . See runs May 11–18 on Table 2. (b) The advance of depth of the mixed layer with time for runs with assorted values of N , one value of R_s , and two values of f . This illustrates the sensitivity of depth with N . See runs May 3–10 on Table 2

and ambient fluid is drawn in to undergo convection. The depth of the mixed layer at this time is consistent with the formula $(B_0R)^{1/3}/N$ in that it is not sensitive to f and is proportional to $B_0^{1/3}/N$.

The mechanism of lateral spreading by the baroclinic eddies strongly resembles the heton mechanism. In the experiment we observed a cyclonic eddy lying over, but laterally offset from, a deeper mass of dyed fluid as found analytically by Crépon *et al.* [1989]. In the numerical experiments we observed cyclonic eddies near the surfaces offset from anticyclonic eddies at greater depths.

In the experiment driven by the paint sprayer, measurements of the velocity, the mode number, and the

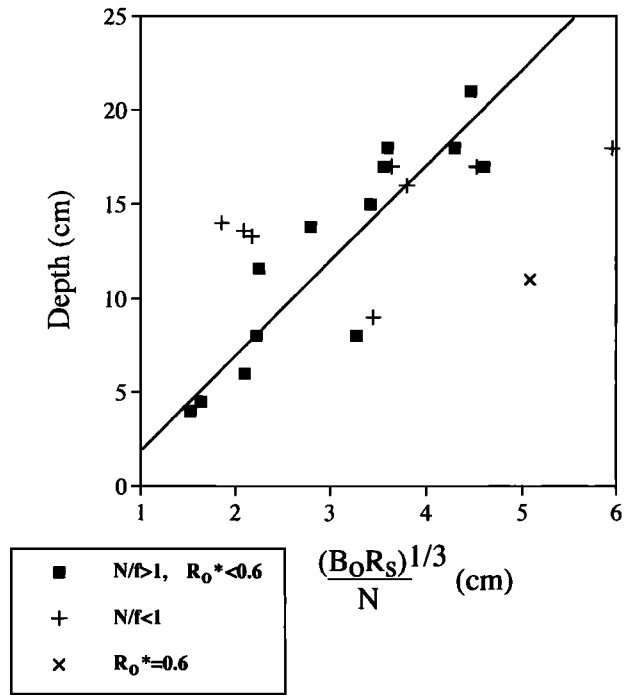


Figure 10. Final mixed layer depth as a function of the depth predicted by (19). The datum with $R_0^* = 0.6$ is shown by a cross; for this case one might expect little baroclinic instability. Data with $N/f < 1$ for which one would expect relatively weak influence of rotation, are shown by pluses. Data with both $N/f > 1$ and $R_0^* = 0.6$, which are most likely to be in the range of validity of the theoretical assumptions behind the scaling arguments, are shown by squares. The least squares fit has a slope of 4.6 and an offset of -1.9 .

eddy size exhibited significant correlation with formulas for these scales from the theory of Visbeck *et al.*, [1996].

In contrast to the paint sprayer experiments, the experiments driven through the diffuser were operated for a full 15 min. In all the experiments, eddies had clearly started to transport density laterally, suggesting that the duration of the experiments was long enough for the scaling to be appropriate. Indeed, the observed depth of the mixed layer had good agreement with the formula in the following ways: depth showed little variation when f was varied with all other parameters held constant; there was dependence on N as predicted; five experiments with the parameter group $B_0^{1/3}/N$ held constant exhibited similar depths even with B_0 varied by 2 orders of magnitude; and finally, experiments with N/f and $R_0^* > 1$ displayed a reasonably linear correlation between depth and our prediction of it.

Perhaps the most significant result is that although the mixed layer deepening is arrested by baroclinic instability, a phenomenon that relies on energy stored in the “thermal wind” and hence reliance on f , the final depth does not depend explicitly on rotation rate. Instead, the final depth of the convectively produced water depends only on the size and intensity of the forcing and the ambient stratification. Implicit in the deriva-

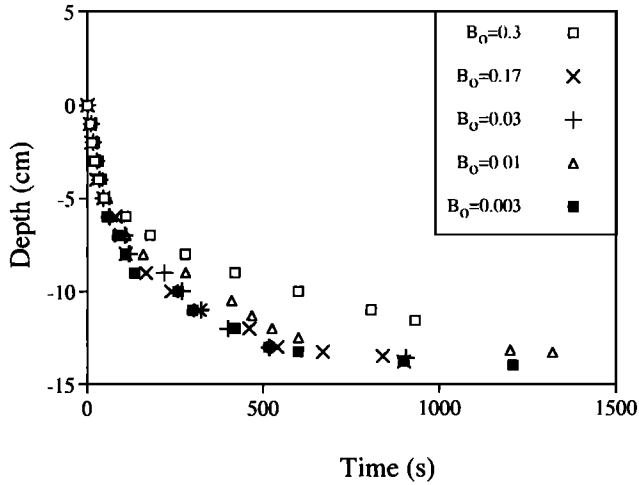


Figure 11. Depth versus time in five experiments where B_0 was varied through 2 orders of magnitude and in which N was adjusted for each run so that depth as predicted by (25) remains constant.

tion of d_s , is the balance between buoyancy forcing at the surface and the lateral transport of dense fluid by baroclinic eddies by the heton mechanism. Again, recall that one of the most important ramifications of the calculated constant of proportionality for depth is an indication of the efficiency of the baroclinic transport. Energy arguments were used in our scaling, assuming that all available potential energy was converted to kinetic energy. The constant of proportionality, 4.6, be-

tween d_r and d_s is a gauge of the efficiency of that process. This balance, then, is important not only in the context of convection but also anywhere that the efficiency of baroclinic eddies is of interest, for example, in the parameterization of baroclinic eddies for use in coarse-scale numerical models.

In the case of convection, where forcing persists long enough for the formation of baroclinic eddies, we propose that the scales summarized below (denoted by “0” in anticipation of their applications to the ocean) will govern the evolution of a convective chimney. The constants of proportionality are deduced from our laboratory experiments in the preceding section.

$$M_0 = 1.0 \frac{R_s^{2/3} f}{B_0^{1/3}} \quad (28)$$

$$v_0 = 0.9(B_0 R_s)^{1/3} \quad (29)$$

$$l_0 = 2.3 \frac{(B_0 R_s)^{1/3}}{f}, \quad (30)$$

$$d_0 = 4.6 \frac{(B_0 R_s)^{1/3}}{N}. \quad (31)$$

To understand when such scaling would be relevant to the ocean we need to take a closer look at the length of time needed for mixed layer deepening to be arrested. Recall that the shortest time necessary for the chimney to evolve to d_{final} is given by

Table 2. Parameters of the Experiments With Steady Forcing.

Date	Diameter cm	f s^{-1}	N s^{-1}	B_0 $cm^2 s^{-3}$	Depth cm	Final N/f cm	R_0^*	$(B_0 R_s)^{1/3}/N$
May 3	15	0.250	0.40	0.30	8	1.6	0.15	3.3
May 4	15	0.250	0.22	0.30	18	0.9	0.15	6.0
May 5	15	0.250	0.86	0.30	4	3.5	0.15	1.5
May 6	15	0.500	0.80	0.30	4.5	1.6	0.05	1.6
May 9	15	0.500	0.38	0.30	9	0.8	0.05	3.4
May 10	15	0.500	0.29	0.30	17	0.6	0.05	4.5
May 11	30	0.250	0.40	0.17	15	1.6	0.11	3.4
May 12	30	0.500	0.36	0.17	16	0.7	0.04	3.8
May 13	30	0.125	0.38	0.17	18	3.0	0.31	3.6
May 16	45	0.500	0.43	0.17	17	0.9	0.04	3.6
May 17	45	0.250	0.34	0.17	17	1.4	0.11	4.6
May 18	45	0.125	0.44	0.17	17	3.5	0.31	3.6
May 20	45	0.250	0.44	0.30	18	1.8	0.15	4.3
May 24	30	0.250	0.37	0.30	21	1.5	0.15	4.5
July 14	45	0.500	0.84	0.30	12	1.7	0.05	2.2
July 15	45	0.500	0.42	0.03	14	0.8	0.02	2.1
July 18	45	0.500	0.22	0.00	14	0.4	0.01	1.9
July 20	45	0.500	0.28	0.01	13	0.6	0.01	2.2
July 21	45	0.500	0.56	0.17	14	1.1	0.04	2.8
July 22	45	0.050	0.19	0.03	11	3.8	0.60	5.1
July 28	45	0.250	0.85	0.27	8	3.4	0.15	2.2
July 29	45	0.125	0.90	0.30	6	7.2	0.41	2.1

$$t = \frac{4}{\sqrt{2}} \left(\frac{R_s^2}{B_0} \right)^{1/3}, \quad (32)$$

using our empirical constant of proportionality for d_{final} and the $\sqrt{2}$ from the one dimensional derivation. Using the following values typical of a Mediterranean convective event, heat flux $\approx 800 \text{ W m}^{-2}$ which, if $\alpha = 10^{-4} \text{ C}^{-1}$, implies $B_0 = 2 \times 10^{-7} \text{ m}^2 \text{ s}^{-3}$ (the actual in situ value is sensitive to temperature and salinity and it is probably less) over an area $R_s = 20\text{--}45 \text{ km}$, we find using (32) that $t = 4 - 7 \times 10^5 \text{ s}$, or $\approx 4\text{--}7$ days. Although the Mistral blows for up to a week, forcing of this magnitude rarely persists for more than 1–2 days. We conclude then that it is unlikely that baroclinic eddies are impacting on the formation of Mediterranean deep water (although they are undoubtedly important in its dispersal once formed). However, the discussion of the duration of the cooling event is subject to so many local factors that further refinement is necessary before being applied to any particular ocean event.

Our estimates can be used to indicate what conditions are needed for deep water formation. Let us take as an example a preconditioned region with a radius of 50 km, $N = 10^{-3} \text{ s}^{-1}$, with $B_0 = 1.25 \times 10^{-7} \text{ m}^2 \text{ s}^{-3}$ (corresponding to a relatively large heat flux of 500 W m^{-2}). We find that d_0 is about 850 m. How could deeper penetration be attained? It is unlikely that B_0 could be significantly larger. However, R_s and N depend on the preconditioning process, so let us examine their effects. To obtain a large increase in predicted depth, for instance by a factor of 2, R_s would need to be 8 times greater, whereas N would only have to be 2 times smaller to get a similar change in depth. Thus the formula indicates that deep convection is sensitive to preconditioning, since gyres of moderate size with lower N are preferred for deep convection compared to larger gyres with larger N .

Now let us consider the Labrador Basin, assuming weather station Bravo to be typical of the entire basin. There is some evidence that the buoyancy flux measured here is representative of the basin based on analyzed fields from European Centre for Medium-Range Weather Forecasting. Then, choosing average winter values from the Bravo records over several years, we find for warm winters a basin-wide heat loss of 100 W m^{-2} , and for extreme cold winters values of 600 W m^{-2} . These heat losses persist for a month or more.

Using an $N \approx 9 \times 10^{-4} \text{ s}^{-1}$ calculated from CTD data stratification encountered by the convective overturning and setting $R_s \approx 100 \text{ km}$ with a heat flux $= 100 \text{ W m}^{-2}$ (implying a $B_0 = 2.5 \times 10^{-8} \text{ m}^2 \text{ s}^{-3}$), (32) gives a depth $d = 695 \text{ m}$ with a minimum formation time of $t = 33.5$ days, long compared with f_0 instability time series. The case of $B_0 = 600 \text{ W m}^{-2}$ corresponds to a final depth $d = 1262 \text{ m}$ and a minimum formation time of $t = 18.5$ days. Note that the stronger the forcing is, the faster the convective penetration and the deeper the mixing is.

The depths predicted above are roughly consistent with recorded depths of mixing at Bravo [Lazier, 1980]. For example, the estimate of 100 W m^{-2} is appropriate to winter 1968, where the recorded depth of mixing was 800 m and we predicted 695 m. Winter 1972 was extremely cold with heat fluxes reaching 800 W m^{-2} . That winter's recorded depth of mixing was 1500 m, where we predicted 1262 m.

Given these estimates it seems likely that Labrador Sea overturning is affected by lateral exchange in baroclinic eddies. In that case, baroclinic eddies formed at the edges of the convection site provide mechanisms for the transfer of convectively produced water into the surrounding water (including the Deep Western Boundary Current (DWBC)).

One might also expect that the final volume of convectively produced water manufactured by one of these events would be governed by the above scaling theories. Labrador Sea Water (LSW) is associated with the (DWBC) as it leaves the Labrador Basin, and transports have been calculated from hydrographic sections through the current. However, very little is known about the frequency, duration, or position of convective events in the Labrador Sea. It is not clear that water with the characteristics of LSW is produced every year; but the signal of LSW associated with the DWBC is relatively steady. In unraveling these questions it will be useful to understand how much water is modified in a given convection event. Such estimates can be made using the ideas here given a hydrographic or survey of the ambient stratification of the region and meteorological surveys of typical storms.

Conclusion

Without doubt, the independence of convection depth from f is interesting and important. It may be surprising to many, and the thorough proof of the scaling theory that leads to this result is not completely straightforward. Perhaps the easiest way to summarize the result is that the velocity of the eddies scales with Nd and that buoyancy scales with N^2d , so buoyancy flux integrated over depth scales as N^3d^3 and that must be integrated around a circumference $2\pi R_s$. In steady state, that flux times circumferential area, must be proportional to buoyancy flux B_0 times surface area, and this leads to the scaling for depth as presented. The entire argument depends on the selection of Nd for the velocity scale and the concept that eddy flux equals velocity scale times buoyancy scale. If the velocity is ultimately driven by the conversion of potential energy into kinetic energy with little dissipation, the above velocity scale would prevail. However, it is possible to argue that other velocity scales could be produced by surface cooling.

However, a variety of data consistent with these scaling relation have been found. Thirty-one laboratory experiments with penetration of a cooled layer into a

rotating stratified fluid produce data that are consistent with the proposed scaling. Nothing has been found at variance. Although the experiments are by no means completely definitive because of scatter from mesoscale variability, we feel that the results provide strong support for the scaling.

Acknowledgments. Support from the Office of Naval Research is gratefully acknowledged. G. H. was supported by an AASERT grant. Support for laboratory experiments were funded by the Ocean Sciences Division of the National Science Foundation under grant OCE92-01464. This is Woods Hole Oceanographic Institution contribution 9104.

References

- Bubnov, B. M., and G. S. Golitsyn, Temperature and velocity field régimes of convective motions in a rotating plane fluid layer, *J. Fluid Mech.*, 219, 215–239, 1990.
- Bubnov, B. M., and A. O. Senatorsky, Influence of boundary conditions on convective stability of horizontal rotating fluid layer, *Izv. Akad. Nauk. SSSR Mekh. Zhidk. Gaza*, 3, 124–129, 1988.
- Chandrasekhar, S., The instability of a layer of fluid heated below and subject to Coriolis forces, *Proc. R. Soc. London A*, 217, 306–327, 1953.
- Chandrasekhar, S., *Hydrodynamic and Hydro Magnetic Stability*, 652 pp, Clarendon, Oxford, 1961.
- Crépon, M., M. Boukthir, B. Barnier, and F. Aikman, Horizontal ocean circulation forced by deep-water, formation. I, Analytical study, *J. Phys. Oceanogr.*, 19, 1781–1793, 1989.
- Davey, M. K., and J. A. Whitehead Jr., Rotating Rayleigh-Taylor instability as a model for sinking events in the ocean, *Geophys. Astrophys. Fluid Dyn.*, 17, 237–253, 1981.
- Eady, E. T., Long waves and cyclone waves. *Tellus*, 1, 33–52, 1949.
- Ellis, H., A letter to the Rev. Dr Hales, *Philos. Trans. R. Soc. London*, 47, 211–214, 1751.
- Fernando, J. S. F., R. Chen, and D. L. Boyer, Effects of rotation on convection turbulence, *J. Fluid Mech.*, 228, 513–548, 1991.
- Gawarkiewicz, G., and D. C. Chapman, A numerical study of dense water formation and transport on a shallow, sloping continental shelf, *J. Geophys. Res.*, 100, 4489–4507, 1995.
- Gill, A. E., J. M. Smith, R. P. Cleaver, R. Hide, and P. R. Jonas, The vortex created by mass transfer between layers of a rotating fluid, *Geophys. Astrophys. Fluid Dyn.*, 12, 195–220, 1979.
- Green, J. S. A., Transfer properties of the large-scale eddies and the general circulation of the atmosphere, *Q. J. R. Meteorol. Soc.*, 96, 157–185, 1970.
- Helfrich, K. R., Thermals with background rotation and stratification, *J. Fluid Mech.*, 259, 265–280, 1994.
- Helfrich, K. R. and T. M. Battisti, Experiments on baroclinic vortex shedding from hydrothermal plumes, *J. Geophys. Res.*, 96, 12,511–12,518, 1991.
- Jones, H., and J. Marshall, Convection with rotation in a neutral ocean: A study of open-ocean deep convection, *J. Phys. Oceanogr.*, 23, 1009–1039, 1993.
- Killworth, P. D., The mixing and spreading phase of MEDOC 1969, in *Progress in Oceanography*, vol. 7, pp. 59–90, Pergamon, Tarrytown, N. Y. 1976.
- Lazier, J. R. N., Oceanographic conditions at ocean weather ship *Bravo*, 1964–1974, *Atmos. Ocean*, 18, 227–238, 1980.
- Legg, S., and J. Marshall, A Heton model of the spreading phase of open-ocean deep convection, *J. Phys. Oceanogr.*, 23, 1040–1056, 1993.
- Madec, G., M. Chartier, P. Delecluse, and M. Crépon, A three-dimensional numerical study of Deep-Water formation in the northwestern Mediterranean Sea, *J. Phys. Oceanogr.*, 21, 1349–1371, 1991.
- Marshall, J., J. A. Whitehead, and T. Yates, Laboratory and numerical experiments in oceanic convection, in *Ocean Processes in climate Dynamics: Global and Mediterranean Examples*, edited by P. Malanotte-Rizzoli and A. R. Robinson, p. 173–201, Kluwer Acad., Norwell, Mass., 1994.
- Maxworthy, T., and S. Narimousa, Vortex generation by convection in a rotating fluid, *Ocean Modell.*, 92, pp. 1007–1008, Hooke Inst., Oxford Univ. Oxford, England, 1991.
- Maxworthy, T., and S. Narimousa, Unsteady, turbulent convection into a homogeneous, rotating fluid, with oceanographic application, *J. Phys. Oceanogr.*, 24, 865–887, 1994.
- Nakagawa, Y., and P. Frenzen, A theoretical and experimental study of cellular convection in rotating fluids, *Tellus*, 7, 1–21, 1955.
- Nansen, F., Northern waters: Captain Roald Amundsen's oceanographic observations of the Arctic Seas in 1901, *Skr. Nor. Vidensk. Akad. Kl. 1 Mat. Naturvidensk.*, Kl., 3, 145 pp, 1906.
- Schott, F., and K. D. Leaman, Observation with moored acoustic Doppler current profiles in the convection régime in the Golfe du Lion, *J. Phys. Oceanogr.*, 21, 558–574, 1991.
- Speer, K. G., and J. Marshall, The growth of convective plumes of seafloor hotspots, *J. Mar. Res.*, 53, 1025–1057, 1995.
- Stommel, H., A. Voorhis and D. Webb, Submarine clouds in the deep ocean, *Am. Sci.*, 59, 717–723, 1971.
- Turner, J. S., *Buoyancy Effects In Fluids*, 368 pp, Cambridge Univ. Press, New York, 1973.
- Veronis, L. D., On properties of sea water defined by temperature, salinity and pressure, *J. Mar. Res.*, 30, 227–255, 1972.
- Visbeck, M. and J. Marshall, and H. Jones 1996. On the dynamics of convective chimneys in the ocean. *J. Phys. Oc.* to appear.

J. A. Whitehead, MS-21, WHOI, Woods Hole, MA 02543 (e-mail: jwhitehead@whoi.edu)

J. Marshall, 54-1526, MIT, Cambridge, MA 02139 (e-mail: Marshall@gulf.mit.edu)

G. Hufford, WHOI, Woods Hole, MA 02543 (e-mail: Gwyneth@gaff.who.edu)

(Received June 26, 1995; revised May 10, 1996; accepted July 25, 1996.)